Journal of Alloys and Compounds 1054 (2026) 186377

Contents lists available at ScienceDirect

Journal of Alloys and Compounds

journal homepage: www.elsevier.com/locate/jalcom

Research Article

Atomic-scale stress release and structure–tribology correlations in alternating-energy DLC films under harsh load conditions

Naizhou Du [a,b], Xin Zhang [c], Xiaowei Li [a,b,*], Kwang-Ryeol Lee [d], Xubing Wei [a], Jiahao Dong [a], Xiang Lu [a], Meng Cheng [a], Peng Guo [b], Kai Chen [a], Dekun Zhang [a], Tiancai Zhang [e,f], Aiying Wang [b,**]

[a] School of Materials Science and Physics, China University of Mining and Technology, Xuzhou 221116, PR China
[b] State Key Laboratory of Advanced Marine Materials, Ningbo Institute of Materials Technology and Engineering, Chinese Academy of Sciences, Ningbo 315201, PR China
[c] Xinhe New Materials (Suzhou) Co., Ltd., Suzhou 215000, PR China
[d] Computational Science Center, Korea Institute of Science and Technology, Seoul 136-791, Republic of Korea
[e] The 11th Research Institute of CSSC, Shanghai 200032, PR China
[f] School of Marine Science and Technology, Northwestern Polytechnical University, Xi'an 710072, PR China

ARTICLE INFO

Keywords:
Diamond-like carbon
Alternating-energy deposition
Friction mechanism
Wear mechanism
Molecular dynamics simulations

ABSTRACT

Diamond-like carbon (DLC) films have attracted significant attention in the field of microscale mechanical components owing to their exceptional tribological properties and chemical inertness. However, the intricate interaction between residual stress and structural integrity poses substantial challenges for their widespread application, particularly under harsh load conditions. This study investigates the deposition and friction behaviors of alternating-energy DLC films under a high contact pressure of 20 GPa using molecular dynamics simulations. By comparing the single- and alternating-energy deposition schemes, this study focuses on the modulation ratio, residual stress distribution, and friction-wear characteristics. The results reveal that alternating-energy deposition significantly reduces residual stress, with values dropping to −3.7 and 0.1 GPa for the 1–70 and 70–1 eV systems, respectively, representing an up to 99 % reduction compared to single-energy deposition. Friction behavior analysis demonstrates that high-energy-terminated deposition systems (70 and 1–70 eV) exhibit low friction coefficients, which was attributed to the formation of a stable, saturated amorphous carbon network at the sliding interface. Quantitative wear rate analysis revealed that the alternating interfacial structure in the alternating-energy deposition system can compromise its wear resistance performance. This study enhances the understanding of DLC multilayer systems under extreme conditions and provides theoretical guidance for the design of stress-relieved and wear-resistant carbon coatings with tailored nanoscale structures.

1. Introduction

Diamond-like carbon (DLC) films have attracted widespread attention as high-performance protective coatings for microscale mechanical components owing to their excellent tribological properties and chemical inertness [1–3]. Their unique structural characteristics—comprising a hybridized network of sp^2- and sp^3-bonded carbon atoms—contribute to their suitability for advanced surface engineering applications, particularly where low friction and chemical stability are essential [4–6]. However, the complex interaction between residual stress and structural integrity poses significant challenges to their widespread application, particularly when operating under harsh load conditions [7–9].

An effective strategy to address these challenges is to modulate the structure of intrinsic DLC films using multilayer structures [10–15]. By alternately stacking layers with different stress states, this multilayer configuration can achieve a stress offset and interrupt the stress network while maintaining ideal friction performance. The alternating layer design provides a way to balance the inherent tradeoffs between hardness, toughness, and stress tolerance. Wang et al. [16] fabricated an

* Corresponding author at: School of Materials Science and Physics, China University of Mining and Technology, Xuzhou 221116, PR China.
** Corresponding author.
E-mail addresses: lixw0826@gmail.com, xwli@cumt.edu.cn (X. Li), aywang@nimte.ac.cn (A. Wang).

https://doi.org/10.1016/j.jallcom.2026.186377
Received 20 November 2025; Received in revised form 4 January 2026; Accepted 21 January 2026

ultra-thick DLC film with a remarkable thickness exceeding 50 μm using the plasma hybrid chemical-physical vapor deposition technique. The film exhibited a sophisticated multilayered architecture of (Si_x-DLC/-Si_y-DLC)$_n$/DLC, where the periodic transition layers consisted of alternately stacked Si-doped DLC sublayers with low and high silicon contents. The compressive stress in the low-silicon-doped layers and the tensile stress in the high-silicon-doped layers counteracted each other, effectively relieving internal stress and resulting in an exceptionally low residual stress of 0.05 GPa. In addition, the ultra-thick DLC film incorporating this periodic transition structure exhibited excellent mechanical performance, including strong film–substrate adhesion (57 N) and high load-bearing capacity (up to 3.2 GPa). However, studies on the performance of multilayer deposition without additional element doping and on the preservation of other intrinsic properties of DLC films are still lacking.

Moreover, the stress and friction responses of DLC film exhibit high sensitivity to multiple factors, including substrate properties, film thickness, and applied contact pressure [17–23]. Notably, recent studies have revealed that under medium-to-high-pressure conditions, the nanostructure and interfacial behavior of DLC films undergo significant modifications compared to low-load scenarios, typically manifesting as nonlinear transitions in both stress distribution and friction mechanisms. For example, Du et al. [24,25] investigated the solid–liquid coupling lubrication behavior between DLC films and PAO lubricants over a wide pressure range. Their work emphasized the transition in the friction mechanism from predominantly hydrodynamic lubrication under low pressure to a competitive regime involving both carbon-hybridized structural evolution and hydrodynamic lubrication under high pressure, demonstrating that this transition process and the resulting friction performance deviated markedly from linear behavior. However, for such a multilayer DLC structure, the accurate extraction of complicated information on the structural evolution of the friction interface is still very challenging yet essential for understanding structure–tribology correlations.

In the absence of in situ experimental characterization methods for deposition and friction processes, molecular dynamics (MD) simulations are an effective approach for analyzing stress fields, bonding environments, and friction responses under highly controlled ideal conditions at the atomic scale [26,27]. Hence, this study used MD simulations to investigate the deposition and friction behavior of a single-period soft-hard alternating DLC film under high-contact pressure conditions. By considering single- and alternating-energy deposition schemes, comparative insights into the modulation ratio, residual stress distribution, and friction and wear were obtained. These results expand the current understanding of DLC multilayer systems under extreme conditions and provide theoretical guidance for the design of stress-relief and wear-resistant carbon coatings with customized nanoscale structures.

2. Computational method

All MD simulations were performed using the LAMMPS package to investigate the deposition and friction behavior of the DLC films modulated by the incident energy [28]. For computational efficiency, both Tersoff and Reactive Force Field (ReaxFF) potentials were considered separately. The Tersoff potential was adopted to describe the interatomic interactions during the deposition stage, with parameterizations specifically optimized for capturing the dynamic transitions between sp^2- and sp^3-hybridized carbon under varying energy conditions [29,30]. This potential has been widely recognized for its success in modeling the bond-rearrangement processes of carbon film growth [31,32]. However, to simulate the friction interactions and interfacial chemical reactions during the subsequent sliding process accurately, the ReaxFF potential parameterized by Tavazza et al. [33] was employed. This potential was extensively validated in our previous work for its ability to capture complex interfacial chemistry and structural evolution under tribological conditions [34–36]. The combined implementation of these two complementary potentials enables a comprehensive exploration of both the energetics and mechanisms governing DLC film growth and tribological performance under operating conditions. In addition, Prior to the friction simulation, the deposited model was relaxed at 300 K for 2.5 ps, during which the atomic configuration was allowed to adapt to the ReaxFF description. This process minimized potential inconsistencies inherited from the Tersoff potential and ensured that the subsequent tribological response was representative within the ReaxFF framework.

2.1. Film deposition

The molecular dynamics simulations employed a diamond (001) slab composed of 3072 carbon atoms and measuring $40.232 \times 40.232 \times 84.779$ Å^3. Periodic boundaries were enforced along the *x* and *y* directions (Fig. 1a). To equilibrate the substrate, the system was maintained at 300 K for 10 ps using the Berendsen thermostat [37]. During deposition, carbon atoms were introduced from a height of 7 nm above the surface with randomized in-plane positions. A three-layer configuration—consisting of fixed, thermostatic, and dynamic regions—was adopted to preserve structural stability while permitting realistic relaxation and growth. Building on the optimal conditions determined in single-energy deposition tests at 1 and 70 eV/atom [31], alternating-energy protocols were implemented. Two modulation strategies were explored: a sequence starting with low-energy deposition followed by high-energy deposition (1–70 eV, low-to-high) and the reverse sequence beginning at high energy then changing to low energy (70–1 eV, high-to-low). For each case, the number of incident atoms was tuned according to optimized modulation ratios to form single-period layered structures. A 10-ps interval between successive impacts was selected to ensure proper structural equilibration (Fig. 1b). To rigorously validate this choice, the evolution of the global system temperature and total kinetic energy was monitored throughout the entire deposition process for various multilayer configurations (Supplementary Information Figure S1). The absence of thermal drift, evidenced by the stable oscillation of temperature around 300 K, confirmed that the 10 ps interval was sufficient to fully dissipate the impact energy of high-energy atoms (70 eV) before the next deposition event. The simulations employed a timestep of 0.25 fs and excluded sputtered atoms to preserve the designed energy conditions. Temperature control was maintained at 300 K throughout the deposition process, and the thermostatic layer was regulated using the Berendsen algorithm. After the deposition stage, the model underwent equilibration at 300 K for 10 ps to ensure thermal relaxation and structural stability. This treatment provided a reasonable representation of the fundamental deposition physics while remaining compatible with the computational limitations inherent to molecular dynamics simulations.

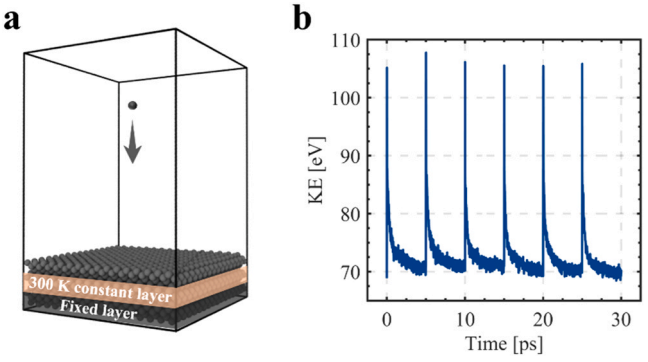

Fig. 1. (a) Substrate model for the deposition process. (b) Evolution of system energy during deposition at an incident energy of 70 eV/atom.

2.2. Friction simulation

To evaluate the tribological response of both multilayer DLC films with varying deposition sequences and single-energy DLC coatings, self-mated sliding models were constructed. Each configuration was partitioned into three regions: a fixed bottom layer, a thermostatted layer for temperature control, and a mobile free layer. Periodic boundary conditions were imposed along the *x* and *y* directions, and the atomic trajectories were integrated using a timestep of 0.25 fs. To emulate harsh load conditions, a contact pressure of 20 GPa was progressively applied to the top amorphous carbon slab, followed by a sliding run of 1250 ps. During this process, the top constrained layer was driven at a uniform velocity of 100 m/s in the *x* direction. Additional parameter settings and methodological details were consistent with those reported in earlier studies [18,19].

3. Results and discussion

3.1. Deposition of DLC films in single- and multilayer configurations

Table 1 summarizes the key deposition conditions applied to the single- and alternating-energy systems. Film thickness was evaluated from density distribution curves using the full width at half maximum approach, and the variation in thickness among different cases was found to be within 8 %. The detailed procedure for defining the effective film thickness is illustrated in Supporting Information Figure S2. The mean density and residual stress distributions were quantitatively evaluated within the defined effective film regions. Notably, the single-energy deposition systems exhibited distinct stress characteristics; deposition at 1 eV resulted in the development of tensile stress, whereas deposition at 70 eV induced compressive stress. This stress transition is governed by distinct growth mechanisms. At 1 eV, the low adatom mobility leads to an island-growth mode, where the coalescence of adjacent atomic clusters generates tensile stress due to attractive grain boundary forces [38]. In contrast, the 70 eV deposition is dominated by the subplantation mechanism; the energetic ions penetrate the subsurface and occupy interstitial sites, creating a dense, over-packed network that exerts strong intrinsic compressive stress on the surrounding matrix [2,39].

The modulation ratio λ was optimized to reduce residual stress in alternating-energy depositions, using the following equations:

$$\lambda = \frac{t_1}{t_2} \tag{1}$$

$$\sigma_{avg} = \frac{\sigma_1 t_1 + \sigma_2 t_2}{t_1 + t_2} \tag{2}$$

where t_1 and t_2 represent the effective thicknesses and σ_1 and σ_2 denote the average stress per unit thickness for depositions carried out at 1 and 70 eV, respectively. Parametric optimization across $\lambda \in [0, 10]$ yielded an optimal ratio of 2.1 that minimized residual stress (Supporting information Figure S3 provides a more detailed calculation process). The alternating-energy configurations 1–70 and 70–1 eV exhibited remarkable stress reduction, with residual stresses measuring −3.7 and 0.1 GPa, respectively, representing an up to 99 % reduction compared to single-energy depositions (Table 1). Notably, the optimal modulation ratio and residual stress values differ from those in previous reports [40], which can be attributed to variations in film thickness. As the film thickness increased, the residual stress decreased [18]. This effect was particularly pronounced in films deposited at 70 eV/atom, where the coupled relaxation of the distorted bond angles and C–C bond lengths facilitated a rapid stress release in thicker films. Complementary density measurements further confirmed the optimized structural characteristics. Although Eq. 2 offers an idealized theoretical prediction by neglecting interfacial transition effects, the results demonstrate that the optimized deposition strategy effectively achieves both substantial residual stress reduction and structural stability.

Table 1
Key parameters obtained from different deposition schemes.

Scheme	Film thickness (Å)	Average density (atoms/Å^3)	Average stress (GPa)
1 eV	36	0.1073	8.37
70 eV	36	0.1477	−17.67
1–70 eV	34.5	0.1280	−3.7
70–1 eV	37.5	0.1225	0.1

Fig. 2a shows the atomic-scale morphologies of the DLC films deposited under different energy conditions, with color coding representing the coordination numbers. The 1 eV/atom deposition yielded a film with pronounced surface roughness, where incident atoms caused minimal substrate disturbance, resulting in a well-defined film–substrate interface. In contrast, the film deposited at 70 eV/atom exhibited a significantly enhanced density and reduced thickness with superior surface smoothness. This morphological transition stems from the incident energy (70 eV) substantially exceeding the cohesive energy of diamond (7.6–7.7 eV/atom) [31], enabling atomic implantation that creates an intermixed interfacial layer. Although this implantation improves the film adhesion, it concurrently generates residual stress by disrupting the crystalline regularity of the substrate.

The 1–70 and 70–1 eV alternating-energy schemes produced layered structures with distinct regions of high and low density. To facilitate comparison between the hard and soft layers, atoms were color-coded in Fig. 2a, with gray representing the hard layers and blue denoting the soft deposition layers. This alternating structure arises from fundamentally different growth mechanisms; the low-energy phase (1 eV) promotes surface adatom configurations with a reduced packing density, whereas the high-energy phase (70 eV) facilitates atomic penetration into the subsurface region, leading to enhanced densification. In the 1–70 eV system, the interlayer interface exhibits pronounced compositional gradients, primarily owing to the looser structure of the underlying 1 eV/atom soft layer, which is attributed to its intrinsic tensile stress characteristics. Subsequent bombardment by high-energy (70 eV) carbon atoms more easily penetrated the deeper regions of the soft layer, promoting extensive interfacial atomic intermixing, and thus forming strong interlayer bonding. In contrast, the 70–1 eV configuration presents sharper layer interfaces with limited atomic interdiffusion between adjacent layers. Despite these interfacial distinctions, both alternating-energy configurations significantly reduced residual stress via two complementary mechanisms: (i) stress compensation between layers of differing densities and (ii) suppression of long-range stress transmission pathways through periodic modulation of the local structure. This nanoscale architectural tuning underscores the crucial influence of energy sequencing on interlayer bonding characteristics and stress distribution in multilayer DLC films.

To quantitatively evaluate the surface morphology, the surface atoms were first identified using the “Construct Surface Mesh” algorithm in OVITO [41]. A probe sphere radius of 3.4 Å and a smoothing level of 8 were employed to accurately distinguish the outermost atoms from the bulk structure without relying on an arbitrary *z*-height threshold. Subsequently, the root mean square (RMS) method was employed to characterize the surface roughness of the DLC films under different deposition conditions. The surface roughness parameter (Rq) was calculated using the following equation:

$$R_q = \sqrt{\frac{\sum_i^N (Z_i - \overline{Z})^2}{N}} \tag{3}$$

where i denotes the atom index, Z_i is the z coordinate of atom i on the deposited film surface, $\overline{Z}$ is the average height of all surface atoms, and N is the total number of surface atoms.

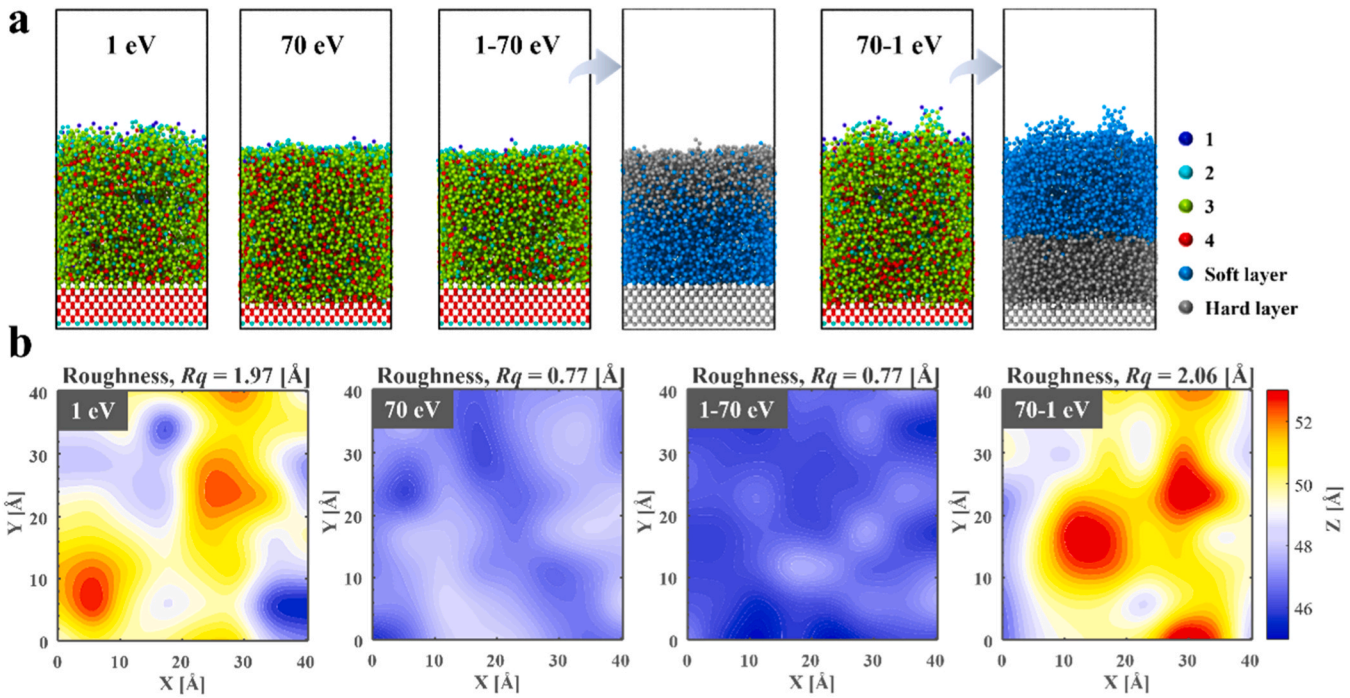

Fig. 2. (a) Coordination configurations of coatings obtained under different incident energies. The color coding represents the coordination numbers. (b) Surface maps and surface roughness (*Rq*) of coatings obtained under different incident energies.

As shown in Fig. 2b, the surface roughness of the film deposited at a low incident energy of 1 eV/atom was significantly greater than that of the film grown at a high incident energy of 70 eV/atom. The corresponding contour plots further highlight the pronounced differences in the surface topography: the low-energy surface exhibits localized protrusions and irregular features, whereas the high-energy surface remains notably smooth. This contrast can be attributed to the distinct surface evolution mechanisms associated with the different incident energies. At low energies, the limited atomic mobility promotes the preferential accumulation of atoms at the surface asperities, thereby amplifying the initial roughness. In contrast, high-energy carbon atoms induce a downhill atomic flow that redistributes surface atoms from elevated regions into adjacent depressions. This energetic redistribution mechanism facilitated the rapid smoothing of the initially rough surface, leading to the formation of a more uniform film morphology [42].

3.2. Structure and stress distributions of single- and multilayer DLC films

The atomic-scale structures of the deposited DLC films were characterized by radial distribution function (RDF) analysis, as shown in Fig. 3a. All the films exhibited characteristic amorphous features. Specifically, the sharp primary peak centered at ~1.5 Å confirms the presence of short-range order corresponding to the nearest-neighbor C–C bond lengths. However, at larger radial distances ($r > 3$ Å), the absence of discrete, periodic peaks and the rapid convergence of *g(r)* to unity indicate a lack of translational symmetry, confirming the long-range disorder of the carbon network. Notably, films deposited at 1 eV/atom displayed additional well-defined peaks at larger interatomic distances, suggesting enhanced medium-range ordering compared with films deposited at higher-energy. The sharp peak observed at approximately 2.1 Å originates from the cutoff radius of the Tersoff potential, commonly referred to as a "false peak" in MD simulations [43,44].

A complementary analysis of the bond length and bond angle distributions (Fig. 3b and c) revealed the atomic-scale mechanisms

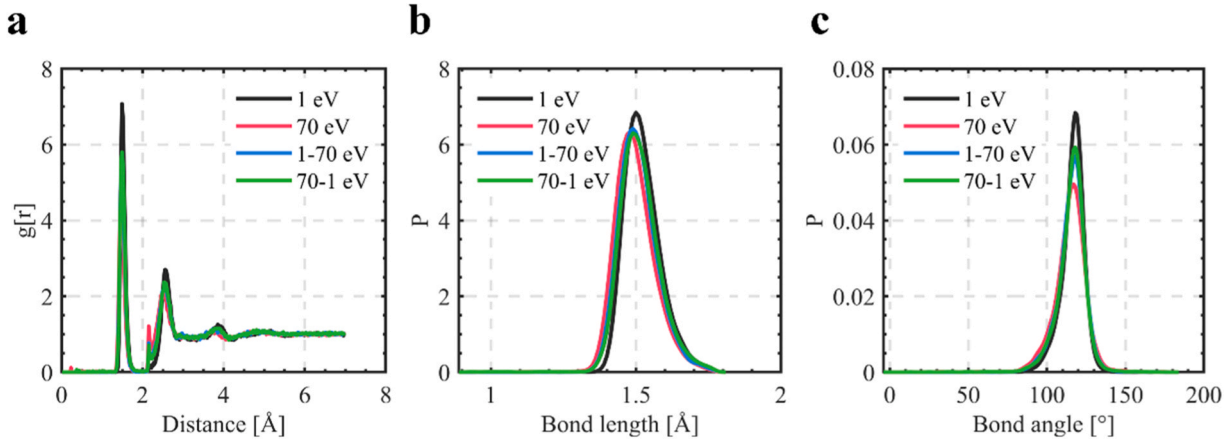

Fig. 3. (a) Radial distribution function. (b) Bond length distribution. (c) Bond angle distribution.

underlying the stress evolution in the deposited films. The bond angle distributions consistently exhibit a dominant peak near 120°, indicative of graphitic sp^2 bonding, confirming the widespread presence of threefold-coordinated carbon atoms across all deposition conditions. However, with increasing incident energy, notable structural variations emerge: the bond angle distribution becomes broader and skews towards smaller angles, reflecting the formation of distorted tetrahedral configurations that are closely associated with the build-up of intrinsic compressive stress. The films prepared under alternating-energy conditions displayed intermediate characteristics, indicating a gradual structural transition modulated by energy alternation. A similar trend was observed for the bond length distributions, which deviated from the ideal C–C bond length value of 1.54 Å. These deviations in the bond lengths and bond angles collectively contribute to the generation of residual stress.

The spatial distribution of the mass density along the z direction (Fig. 4) reveals three distinct structural regions that demonstrate a clear dependence on the incident energy: (i) the substrate region maintaining a complete diamond lattice, (ii) the initial effective film thickness region showing gradual amorphization, and (iii) the surface region dominated by unsaturated carbon. Notably, in the 70 and 70–1 eV systems, the film–substrate interface exhibit pronounced structural gradients, characterized by a gradual decrease in mass density and sp^3 content accompanied by a corresponding increase in the sp^2 fraction (Supporting Information Figure S4). This gradient originates from the enhanced atomic penetration and extensive intermixing induced by the high incident energy, resulting in a broader interfacial transition zone and partial disruption of the diamond lattice structure. In the surface region, elevated sp hybridization was consistently observed owing to the termination of the carbon network, with the unsaturation levels inversely correlated with the incident energy (Supporting Information Figure S4).

Alternating-energy deposition (1–70 and 70–1 eV) resulted in a distinct modulation structure in both the mass density and hybridized states (Fig. 4). These systems exhibit synchronized oscillations in sp^3 content and mass density, accompanied by reverse variations in sp^2 and sp fractions, highlighting the effectiveness of energy modulation in spatially tailoring local bonding environments (Supporting Information Figure S4). Across all films, the sp^3 fractions remain within a constrained range (15–30 %), which partially reflect the intrinsic limitations of the Tersoff potential in accurately capturing the complex bonding in highly disordered carbon networks [30]. Quantitative hybridization analysis (Fig. 5) further confirmed the structural intermediacy of alternating-energy systems, with both density and sp^3 content positioned between those of the porous, sp^2-rich 1 eV films and the dense, sp^3-rich 70 eV films (Supporting Information Figure S5). This tunable hybridization and density profile underscores the potential of alternating-energy strategies to mitigate excessive residual stress.

Fig. 6 shows the residual-stress distribution along the z direction, revealing distinct energy-dependent characteristics. In the 1 eV/atom deposited films, a distinct transition is evident, shifting from compressive stress in the substrate to tensile stress in the stabilized film region. In contrast, the 70 eV/atom deposition produced uniform compressive stress throughout the film thickness, resulting from both implantation-induced densification and the formation of distorted tetrahedral bonds. Notably, a pronounced compressive stress is observed in the transition zone connecting the substrate and the film body, significantly exceeding that of the stabilized film region. This stress concentration is likely a key driver of delamination behavior.

The alternating-energy deposition method (1–70 and 70–1 eV) produces a single-period opposite stress distribution that oscillates between the tensile and compressive states in synchronization with the energy modulation. This stress distribution can achieve an effective compensation mechanism in which adjacent layers with opposite stress states cancel out their residual stresses. The significant reduction in the residual stress compared with single-energy deposition was due to the prevention of large-scale stress network formation by continuously interrupting the stress propagation path.

3.3. Comparison of frictional responses in single- and multilayer DLC films

To comprehensively investigate the tribological behavior of various DLC deposition systems under high contact pressure and to elucidate the structure–property relationships governing their friction performance, particularly the unique characteristics of alternating-energy deposited films, self-mated friction configurations using identical DLC film models were constructed (Fig. 7).

Fig. 8a shows the evolution of friction forces of the four distinct DLC deposition systems during sliding under a contact pressure of 20 GPa, revealing a pronounced running-in period (~100 ps) characterized by an initial rise in friction followed by stabilization. Notably, the 70 eV system exhibited distinct behavior, with a sharp initial friction peak that subsequently decreased significantly. This trend results from the interplay between the interfacial C–C covalent bond formation—driven by dangling bond interactions, which temporarily enhances shear resistance—and the rapid development of a saturated carbon hybridization network that suppresses further bond formation and reduces friction [45,46]. The dense atomic structure and elevated sp^3 content of the 70 eV film promote the early formation of a stable interfacial network, enabling faster friction stabilization compared with the more porous, low-energy-deposited counterparts. This interfacial restructuring underscores the critical role of deposition energy-controlled surface chemistry in dictating the tribological performance of films (Supporting Information Figure S6).

The average friction forces and normal loads during the stable sliding period (final 200 ps) revealed distinct load-bearing capacities and friction responses across the different deposition systems (Supporting

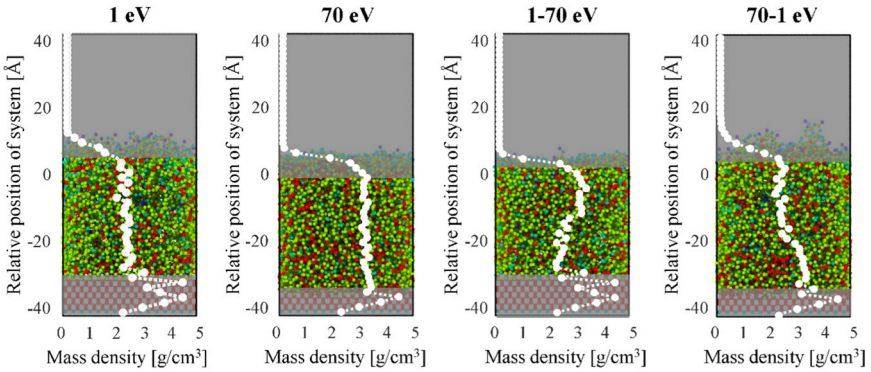

Fig. 4. Distribution of the mass density of different deposition systems.

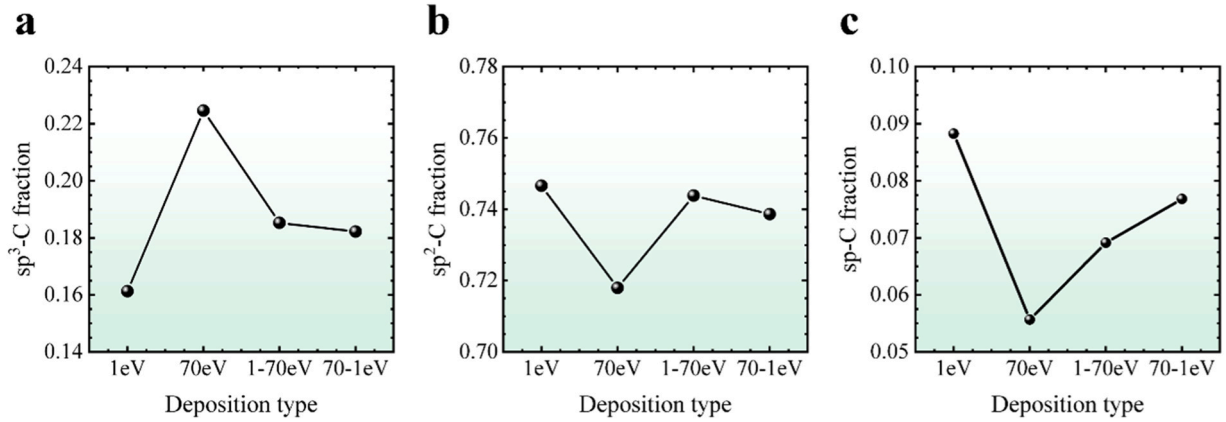

Fig. 5. Hybridized structures of different deposition systems.

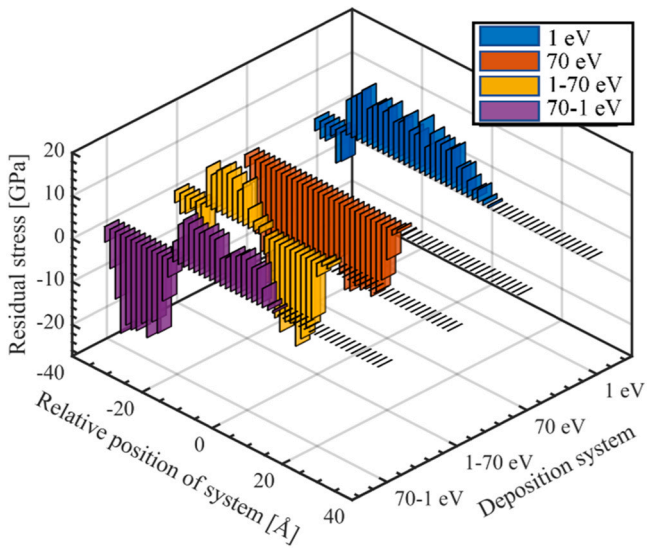

Fig. 6. Stress distribution along the z direction under different incident energies.

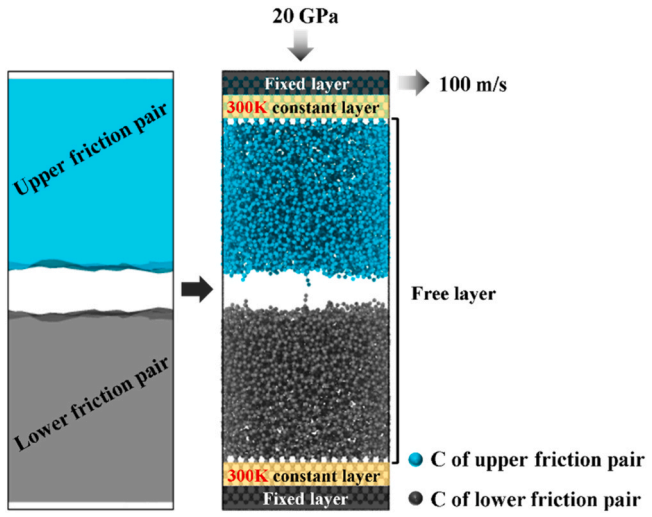

Fig. 7. Friction pair constructed model of the 1–70 eV deposition system.

Information Figure S7). The 70 eV system demonstrates superior load-bearing ability, attributed to its dense, highly cross-linked amorphous carbon structure with elevated sp^3 content. In contrast, the 1–70 eV system shows intermediate performance owing to the structural compromise between its dense top layer (70 eV) and porous bottom layer (1 eV), while both the 1 and 70–1 eV systems exhibit significantly reduced load-bearing capacity resulting from their predominant sp^2-rich, loose architectures (Supporting Information Figure S5). For every simulated system, the value of the friction coefficient (μ) was obtained using the following equation:

$$\mu = \frac{f}{W} \tag{4}$$

where f is the average friction force and W refers to the normal load, both averaged over the final 200 ps of steady sliding. The 70 and 1–70 eV systems exhibit lower friction coefficients (μ = 0.789 and 0.927, respectively) compared to the 1 and 70–1 eV systems (μ = 1.336 and 1.186, respectively) (Fig. 8b). This enhanced tribological performance is correlated with the presence of high-energy carbon atoms deposited at the sliding interface, which form a stable, saturated amorphous carbon network that effectively minimizes adhesive interactions and shear resistance [47]. It should be emphasized that the friction coefficients reported herein are systematically higher than the values typically observed in experimental studies [19]. The primary reason for this deviation lies in the simulation setup, which employed idealized amorphous carbon surfaces without passivation. Consequently, effects such as surface contamination, adsorbed species, and other environmental influences—commonly present in real experimental conditions—were not captured in the MD simulations.

The origins of the tribological behavior in alternating-energy-deposited films were investigated through a systematic analysis of their morphological evolution during sliding. As shown in Fig. 9, the color-coded interacting counterfaces at 20 GPa reveal two distinct phenomena: progressive densification occurs in the 1 eV/atom regions through the collapse of their intrinsic porous structure (Supporting Information Figure S5), whereas extensive interfacial C–C covalent bond formation becomes particularly evident in the 70 eV system. The pronounced bonding behavior originates from the inherently high sp^3-hybridized carbon content and abundant surface dangling bonds characteristic of this system (Supporting Information Figure S5). Interestingly, although pressure-dependent graphitization has been reported in dual-period soft-hard alternating systems at 5 GPa [40], such layered graphitic structures become negligible at 20 GPa. This transition suggests the existence of a critical pressure threshold, where the structural evolution is dominated by the combined effects of the loading conditions, modulation periodicity, and film thickness.

The observed interfacial C–C bonding behavior directly correlated with significant changes in the atomic coordination states, as revealed by coordination number mapping and distribution analysis (Fig. 9). The

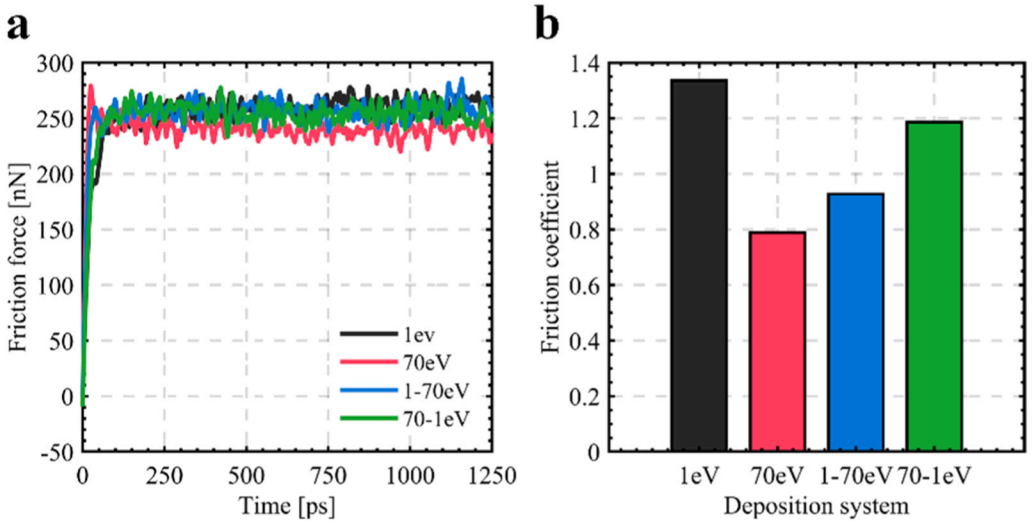

Fig. 8. (a) Temporal evolution of friction forces during sliding. (b) Friction coefficient of different deposition systems.

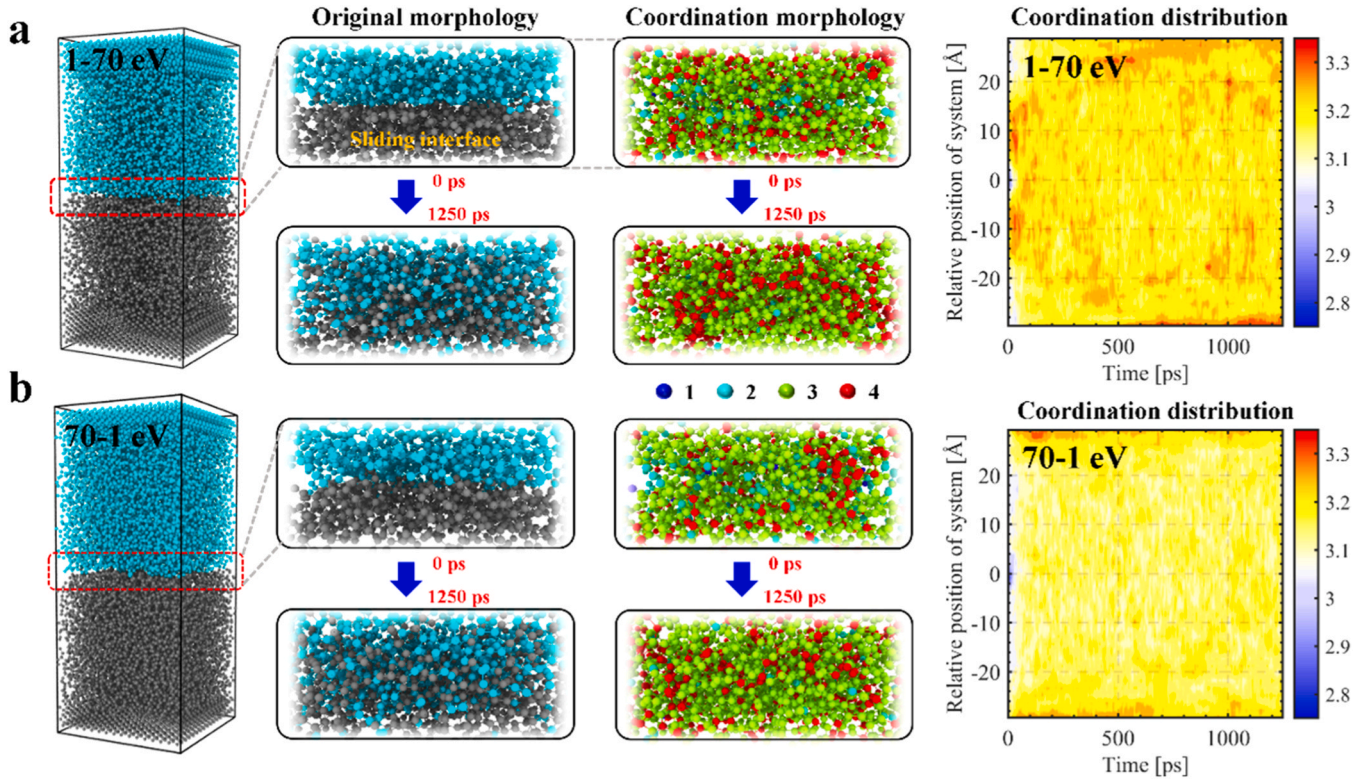

Fig. 9. The original morphology and coordination number morphology of the friction interface in the (a) 1–70 and (b) 70–1 eV systems, as well as the evolution of the coordination number distribution in the systems.

sliding interface undergoes rapid transformation from an initially unsaturated state (dominated by sp-hybridized carbon) to a complex 3D network of sp^2- and sp^3-hybridized carbon, with this transition completing within the running-in period (~100 ps) of the friction curve. This reconstruction process is particularly enhanced in the high-energy surface systems (70 and 1–70 eV), where carbon atoms exhibit a stronger coordination saturation trend (Supporting Information Figure S8), as evidenced by the higher sp^3 content in the coordination morphology of the 1–70 eV system at the end of sliding.

The mass density distributions (Fig. 10a) reveal the complex structural evolution during sliding in the different deposition systems. In the single-energy systems, densification occurs in the initially loose 1 eV system, as evidenced by the aforementioned morphological and coordination distributions. For the 70 eV system, although interfacial C–C covalent bonding increases the density at the sliding interface, shear-induced atomic rearrangement leads to the homogenization of the initially dense bulk structure. These structural changes are closely correlated with stress redistribution (Fig. 10b): the 1 eV system exhibits increased compressive stress under load owing to densification, while the 70 eV system achieves stress homogenization, alleviating the deep-layer stress concentration observed under static conditions.

In the alternating-energy systems, friction weakens the original soft-hard stratified structures via distinct mechanisms. In the 1–70 eV configuration, the bottom soft layer (1 eV) acted as a buffer layer that

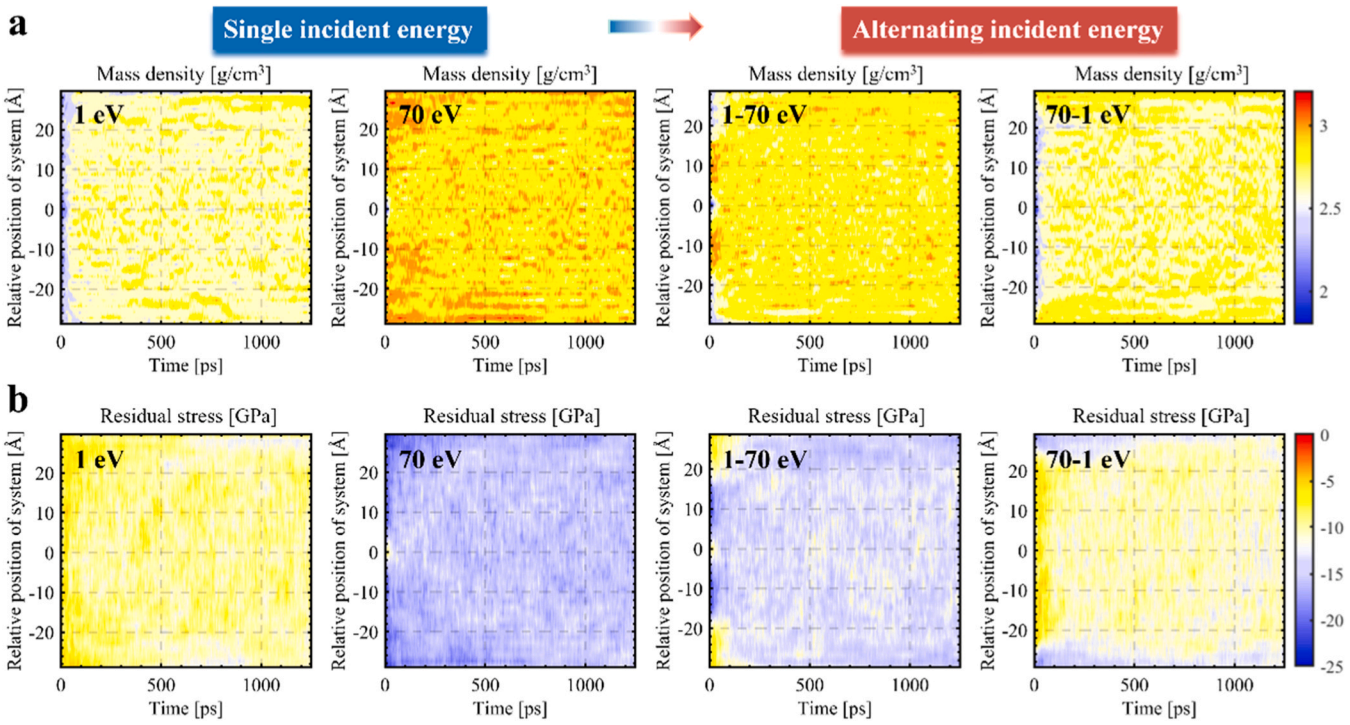

Fig. 10. (a) Mass density distribution and (b) residual stress distribution of different deposition systems during the friction process.

lost its low-density characteristics under the combined normal and shear stresses, causing a rapid increase in stress during the initial running-in period (~100 ps). In contrast, the 70–1 eV system primarily undergoes friction-induced densification in the top soft layer (1 eV), whereas the underlying hard layer (70 eV) largely maintains its high-density and high-stress distribution. This structural asymmetry highlights the critical role of the deposition sequence in controlling friction reorganization within nanolayered DLC films.

Fig. 11 shows the friction-induced evolution of the hybridized structures in the different deposition systems. The 70 eV system exhibited the highest sp^3-hybridized carbon content, because of the dense structure formed by the high incident energy, followed by the 1–70 eV system, whereas the 1 and 70–1 eV systems have lower sp^3-hybridized carbon content at the friction interface. Notably, consistent with the density distribution during the friction process, the sp^3 content in the systems tended to be more uniformly distributed along the *z* direction. Specifically, low incident energy systems form numerous C–C bonds during friction, thereby increasing the amount of saturated amorphous carbon. In high-incident energy systems, where sp^3-hybridized carbon is initially concentrated in the upper and lower friction pairs, the shear forces during friction led to a homogeneous distribution at the friction interface. In the alternating-energy deposition systems, the sp^3 distribution maintains a hard-soft alternating state at the early stage of friction, especially in the 1–70 eV system. However, as friction progressed, the sp^3-hybridized carbon in the hard surface layer was redistributed towards both the hard and soft regions under high pressure. In the 70–1 eV system, because tribochemical reactions predominantly occur in the soft surface layer with minimal impact on the hard bottom layer, the sp^3-hybridized carbon at the friction interface does not diffuse as deeply as in the 1–70 eV system. Overall, the sp^3-hybridized carbon content of the different deposition systems increased to varying degrees after sliding; however, the order of the sp^3-hybridized carbon content among these systems remained unchanged. This indicates that even under high pressure, alternating-energy deposition systems can maintain excellent tribological performance despite the partial densification of the soft surface layer.

Regarding sp^2 hybridization, because the internal structure of the DLC films is mainly composed of sp^3- and sp^2-hybridized carbon, a mutual transformation occurs during the friction process. In the 1 eV system, sp^2-hybridized carbon significantly accumulated at the friction interface, whereas in the 70 eV system, sp^2-hybridized carbon diffused towards both ends. Intriguingly, in the 1–70 eV system, sp^2-hybridized carbon in the hard surface layer diffused towards both ends, whereas sp^2-hybridized carbon in the soft buffer layer concentrated at the friction interface, resulting in a homogeneous distribution of hybridized structures (including sp^3 and sp^2) at the end of friction. In contrast, the 70–1 eV system mainly relies on the soft surface layer for structural evolution during friction. In addition, because the sp-hybridized carbon content was relatively low, it largely transformed into sp^2 and sp^3-hybrided carbon under high-pressure friction. Notably, in the 1 and 70–1 eV systems, as the friction interface is dominated by the loose soft layer, the conversion ratio of sp content during friction is higher.

Fig. 11b shows the hybridized content before and after friction, demonstrating the contribution of sp to the formation of sp^2 and sp^3 during the friction process. In the 1 eV system, sp mainly transforms into sp^2. However, compared to previous friction studies under low pressure, the significant increase in sp^2 content did not lead to the formation of obvious graphite-like layered structures, suggesting that the sp^2-hybridized carbon formed during the friction process mainly constitutes C–C bonds that impede shear motion, resulting in a higher friction coefficient. In the 70 and 1–70 eV systems, the friction process was dominated by the hard surface layer. The limited transformation of the relatively small amount of sp-hybridized carbon mainly results in sp^3 hybridization. This indicates that the hybridization distribution during friction is mainly attributable to the mutual transformation between sp^2- and sp^3-hybridized carbon, leading to a homogeneous distribution. The formation of saturated amorphous carbon implies an increase in the degree of passivation at the friction interface. The lack of active sites in saturated amorphous carbon reduces its resistance to shear during friction, resulting in a relatively low friction coefficient. Although the 70–1 eV system also experienced a significant transformation of sp into sp^3, the hard layer in its alternating structure did not participate in the friction evolution process to a great extent. The positive effect of the passivation of the soft surface layer fails to significantly change the fact

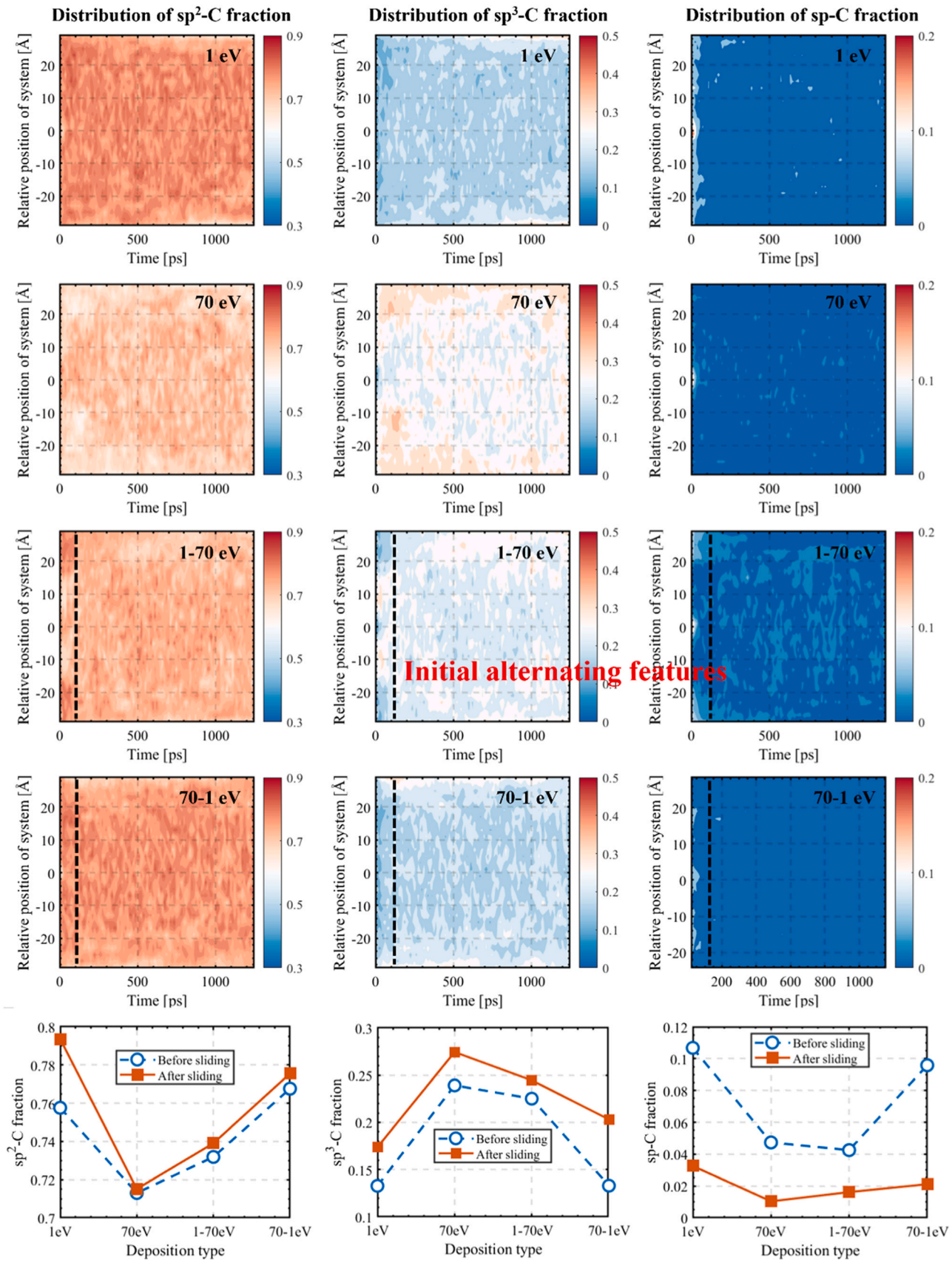

Fig. 11. (a) Hybridized structure distribution of different deposition systems during the friction process. (b) Hybridized structure fraction of different deposition systems before and after sliding.

that the content of saturated carbon hybridization is inherently low, resulting in a slightly higher friction coefficient compared with that of the 1–70 eV system.

3.4. Comparison of wear behavior in single- and multilayer DLC films

Atomic-scale wear differs fundamentally from macroscopic wear, as chemical reactions and interfacial interactions dominate the tribological behavior rather than bulk material properties such as strength and hardness [48]. However, understanding the interfacial reactions and atomic-scale wear mechanisms presents significant challenges. The most widely accepted atomic-scale wear model employs a ball-on-disk configuration in which a rigid spherical counterface slides against a flat substrate or coating [49]. This approach allows the quantification of wear through the analysis of two/three-dimensional topographic profiles, similar to experimental measurements. However, this model cannot adequately simulate lubrication conditions involving liquid lubricants, water molecules, or gaseous environments. Alternatively, Wang et al. [50] developed a hydrogenated amorphous carbon model with semicircular protrusions to study the triboemission of hydrocarbon molecules, defining chemical wear as hydrocarbon release and adhesive wear as interfacial C–C bond formation.

In self-mated sliding systems, research has primarily focused on friction behavior, whereas wear characterization remains less defined. The presence of surface dangling bonds in amorphous carbon leads to extensive interfacial crosslinking. Previous studies [25] have quantified this wear-like behavior using a bonding ratio (the fraction of newly formed C–C bonds relative to the total number of atoms), which provides a reasonable but simplified representation of wear. Herein, we implemented a more direct quantification method by physically separating the counterfaces after sliding. The high strength of C–C covalent bonds enables this approach.

The separation procedure involved: (1) unloading the 20 GPa contact pressure over 25 ps, followed by (2) applying a 5 m/s upward velocity to the upper fixed layer for 100 Å displacement (Fig. 12a). This process generated elongated C–C chains between the separated surfaces, although their influence on the wear quantification was negligible because of the sufficient separation distance. Material transfer between counterfaces was clearly observed, with notable differences between systems: the single-energy systems showed symmetric transfer, whereas alternating-energy systems exhibited asymmetric transfer, likely due to soft-hard interface effects.

Mass density distribution analysis during unloading (Fig. 12b and Supporting Information Figure S9) revealed uniform density changes in the single-energy systems, compared to significant gradients in alternating-energy systems. The 1–70 eV system lost its layered structure, while the 70–1 eV system maintained a high-density bottom layer. The wear rate was quantified as the ratio of the number of transferred atoms to the total number of system atoms (Fig. 12c). The single-energy systems demonstrated lower wear rates, with the 70 eV system showing exceptional resistance (wear rate = 0.062), consistent with conventional hardness–wear relationships. Although high-pressure sliding homogenized the soft-hard layers in the alternating-energy systems, their wear behavior fundamentally differed from that of the single-energy systems. Weaker bonding at the homogenized soft-hard interfaces became apparent during separation, leading to higher wear rates, particularly for the 70–1 eV system, where the initially distinct interfaces (Fig. 2) ultimately compromised the wear resistance.

As shown in Fig. 13, the Pearson correlation analysis revealed significant structure–property relationships in the investigated DLC systems. Density showed a near-perfect positive correlation with sp^3 content ($r = 0.989$) and strong negative correlation with sp^2 content ($r = -0.900$), confirming the fundamental relationship between film densification and carbon hybridization states. Residual stress had an exceptionally strong negative correlation with wear rate ($r = -0.948$), highlighting that the stress state directly influences wear resistance. The

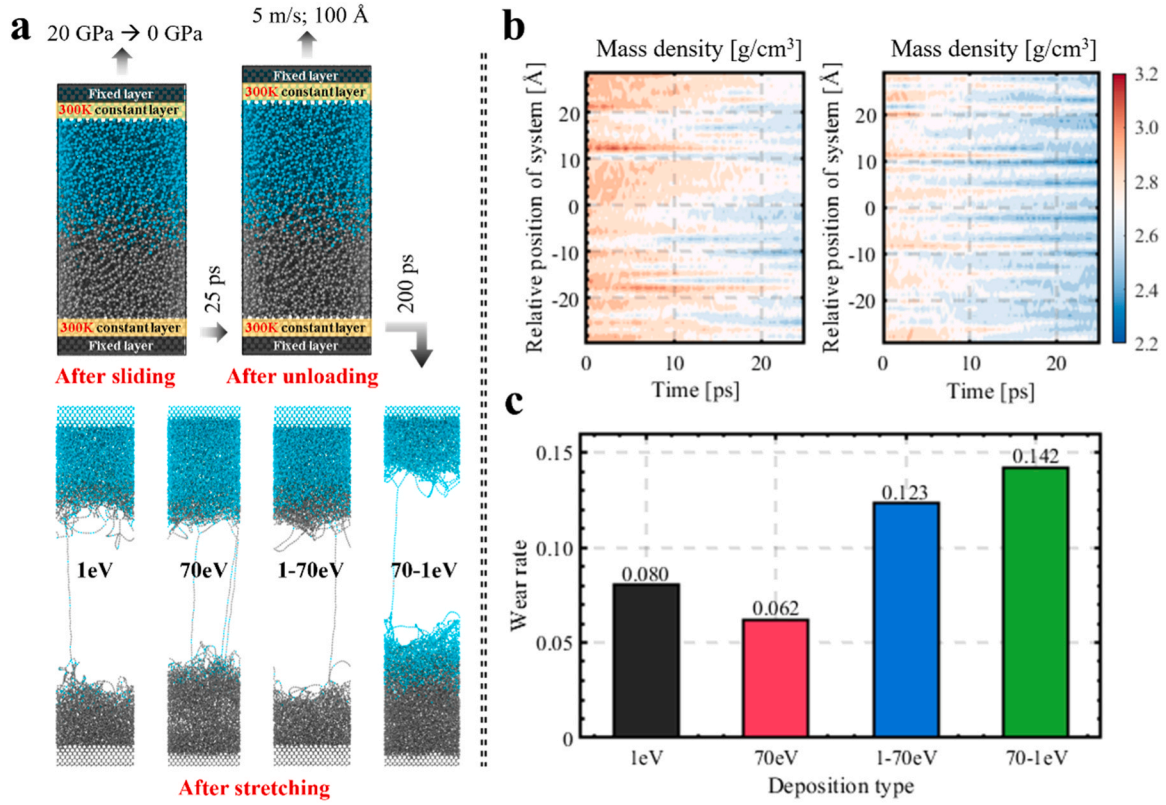

Fig. 12. (a) Schematic of the unloading-stretching process and morphology of different deposition systems after stretching. (b) Mass density distribution of the alternating-energy systems during the unloading process. (c) Wear rate.

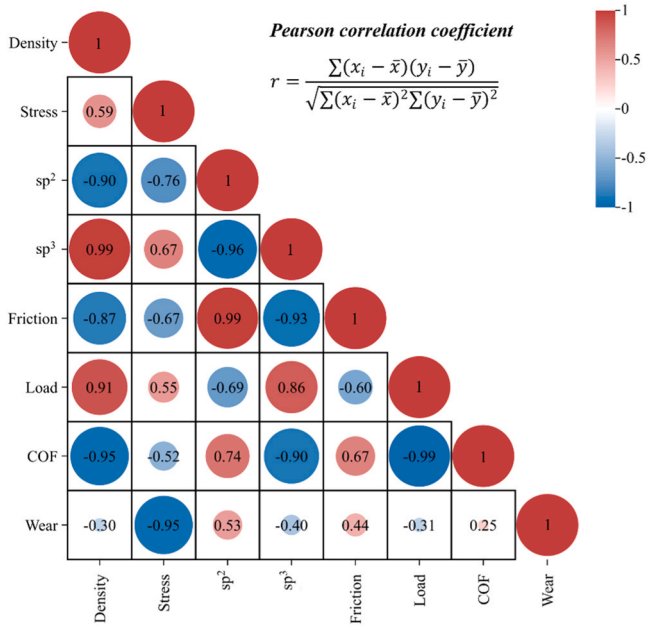

Fig. 13. Pearson correlation coefficient of structure–property relationships.

Pearson correlation analysis revealed distinct tribological behavior patterns. While the sp^2 content exhibited a remarkably strong positive correlation with friction ($r = 0.988$), its correlation with the wear rate was substantially weaker ($r = 0.527$). This decoupling indicated that friction and wear were governed by different mechanisms in these systems. The coefficient of friction exhibits a near-perfect negative correlation with applied load ($r = -0.992$), demonstrating extreme pressure sensitivity in the friction response.

Notably, several moderate correlations provided additional insights. The positive correlation between density and applied load ($r = 0.909$) suggested pressure-induced densification effects, while the negative correlation between sp^3 content and friction ($r = -0.926$) confirmed the role of diamond-like bonding in friction reduction. The relatively weak correlations involving the wear rate (absolute values <0.53 except for stress) indicate that the wear behavior depends on more complex interactions between multiple factors.

Collectively, these correlation patterns demonstrate that, while carbon hybridization states primarily govern friction properties, residual stress plays a dominant role in wear resistance. These results suggest that optimizing the DLC film performance requires balancing these competing structural characteristics, particularly for applications involving high contact pressures.

4. Conclusion

This study utilized MD simulations to elucidate the stress release, friction, and wear mechanisms of alternating-energy DLC films under high contact pressure (20 GPa). The key findings provide theoretical guidance for balancing the trade-offs in DLC films design:

- **Stress Reduction Mechanism:** Alternating-energy deposition achieves a substantial residual stress reduction (up to 99 %) via a stress compensation mechanism. The alternation between tensile-stressed (soft) and compressive-stressed (hard) layers effectively interrupts long-range stress transmission pathways, offering a superior strategy for stress management compared to single-energy deposition.
- **Tribological performance:** The high-energy surface termination promotes the rapid formation of a stable, saturated amorphous carbon network at the sliding interface. This structural evolution transitions the friction mechanism from adhesion-dominated to homogeneous shear, resulting in significantly reduced friction coefficients for the alternating systems.
- **Wear mechanisms:** While alternating structures excel in stress relief, their wear resistance is influenced by interfacial integrity. The chemical gradient at the soft-hard interface can compromise bonding strength, leading to asymmetric wear behavior. A strong negative correlation between residual stress and wear rate confirms that retaining some compressive stress is essential for wear resistance.
- **Structure–property relationships:** Mass density correlated strongly with sp^3 content ($r = 0.989$) and residual stress, whereas sp^2 content significantly influenced friction ($r = 0.988$). These relationships underscore the importance of carbon hybridization and the stress state in tailoring the performance of DLC film.

CRediT authorship contribution statement

Xiang Lu: Writing – original draft, Formal analysis. **Meng Cheng:** Writing – original draft, Formal analysis. **Peng Guo:** Writing – original draft, Formal analysis. **Kai Chen:** Writing – original draft, Formal analysis. **Dekun Zhang:** Writing – original draft, Formal analysis. **Tiancai Zhang:** Writing – original draft, Formal analysis. **Naizhou Du:** Writing – original draft, Visualization, Methodology, Investigation, Formal analysis, Data curation, Conceptualization. **Aiying Wang:** Writing – review & editing, Supervision, Resources, Conceptualization. **Xin Zhang:** Writing – original draft, Formal analysis. **Xiaowei Li:** Writing – review & editing, Writing – original draft, Supervision, Resources, Investigation, Funding acquisition, Data curation, Conceptualization. **Kwang-Ryeol Lee:** Writing – review & editing, Supervision, Resources, Conceptualization. **Xubing Wei:** Writing – original draft, Formal analysis. **Jiahao Dong:** Writing – original draft, Formal analysis.

Declaration of Competing Interest

The authors declare that they have no known competing financial interests or personal relationships that could have appeared to influence the work reported in this paper.

Acknowledgments

This research was supported by the National Natural Science Foundation of China (No. U24A2030, No. 52175204) and Xuzhou “343” Industrial Development Project (No. gx2025006).

Appendix A. Supporting information

Supplementary data associated with this article can be found in the online version at doi:10.1016/j.jallcom.2026.186377.

References

[1] K. Holmberg, A. Erdemir, Influence of tribology on global energy consumption, costs and emissions, Friction 5 (3) (2017) 263–284.
[2] J. Robertson, Diamond-like amorphous carbon, Mater. Sci. Eng. R. Rep. 37 (4-6) (2002) 129–281.
[3] X. Wei, S. Shi, C. Ning, et al., Si-DLC films deposited by a novel method equipped with a co-potential auxiliary cathode for anti-corrosion and anti-wear application, J. Mater. Sci. Technol. 109 (2022) 114–128.
[4] K. Bewilogua, D. Hofmann, History of diamond-like carbon films - from first experiments to worldwide applications, Surf. Coat. Technol. 242 (2014) 214–225.
[5] B. Shi, Y. Wu, Y. Liu, et al., A review on diamond-like carbon-based films for space tribology, Mater. Sci. Technol. 38 (15) (2022) 1151–1167.
[6] Z. Han, H. Li, G. Lin, et al., Influence of nitrogen flow rate on the microstructure and properties of N and Me (Me=Cr, Zr) co-doped diamond-like carbon films, J. Mater. Sci. Technol. 26 (11) (2010) 967–972.
[7] F.O. Kolawole, O.S. Kolade, S.A. Bello, et al., The improvement of diamond-like carbon coatings for tribological and tribo-corrosion applications in automobile engines: an updated review study, Int. J. Adv. Manuf. Technol. 126 (5-6) (2023) 2295–2322.
[8] X. Li, P. Guo, L. Sun, et al., Ti/Al co-doping induced residual stress reduction and bond structure evolution of amorphous carbon films: an experimental and ab initio study, Carbon 111 (2017) 467–475.

[9] Y.T. Li, X.M. Chen, X.K. Zeng, et al., Hard yet tough and self-lubricating (CuNiTiNbCr)Cx high-entropy nanocomposite films: effects of carbon content on structure and properties, J. Mater. Sci. Technol. 173 (2024) 20–30.
[10] J. Wei, H. Li, L. Liu, et al., Enhanced tribological and corrosion properties of multilayer ta-C films via alternating sp^3 content, Surf. Coat. Technol. 374 (2019) 317–326.
[11] Z. Xu, H. Sun, Y.X. Leng, et al., Effect of modulation periods on the microstructure and mechanical properties of DLC/TiC multilayer films deposited by filtered cathodic vacuum arc method, Appl. Surf. Sci. 328 (2015) 319–324.
[12] M.S. Kabir, Z. Zhou, Z. Xie, et al., Designing multilayer diamond like carbon coatings for improved mechanical properties, J. Mater. Sci. Technol. 65 (2021) 108–117.
[13] Y. Lin, A.W. Zia, Z. Zhou, et al., Development of diamond-like carbon (DLC) coatings with alternate soft and hard multilayer architecture for enhancing wear performance at high contact stress, Surf. Coat. Technol. 320 (2017) 7–12.
[14] Y. Lin, Z. Zhou, K.Y. Li, Improved wear resistance at high contact stresses of hydrogen-free diamond-like carbon coatings by carbon/carbon multilayer architecture, Appl. Surf. Sci. 477 (2019) 137–146.
[15] Z. Huang, W. Tian, J. Wang, et al., Planification of amorphous carbon coatings via periodically transitional sp2/sp3 bonds to enhance cavitation erosion resistance, Carbon 230 (2024) 119641.
[16] J. Wang, J. Pu, G. Zhang, et al., Interface architecture for superthick carbon-based films toward low internal stress and ultrahigh load-bearing capacity, ACS Appl. Mater. Interfaces 5 (11) (2013) 5015–5024.
[17] C. Wei, J. Yang, F. Tai, The stress reduction effect by interlayer deposition or film thickness for diamond like carbon on rough surface, Diam. Relat. Mater. 19 (5-6) (2010) 518–524.
[18] X. Li, S. Xu, P. Ke, et al., Thickness dependence of properties and structure of ultrathin tetrahedral amorphous carbon films: a molecular dynamics simulation, Surf. Coat. Technol. 258 (2014) 938–942.
[19] Z. He, P. Shi, X. Zhong, et al., Friction condition switching two-type transfer layers of hydrogenated amorphous carbon with distinct tribological behaviors, Carbon 238 (2025) 120198.
[20] H. Sun, Z. Li, D. Wang, et al., Friction reduction and wear mechanisms of Si-DLC film in humid environment: a ReaxFF MD study, Diam. Relat. Mater. 154 (2025) 112186.
[21] R. Zhang, Q. Chen, Z. He, et al., In situ friction-induced amorphous carbon or graphene at sliding interfaces: effect of loads, Appl. Surf. Sci. 534 (2020) 146990.
[22] Y. Jang, J. Kim, W. Lee, et al., Tribological properties of multilayer tetrahedral amorphous carbon coatings deposited by filtered cathodic vacuum arc deposition, Friction 9 (5) (2021) 1292–1302.
[23] G. Ma, J. Yan, N. Lin, et al., Manipulation of Cr interlayer in amorphous carbon coating for anti-tribo-corrosion behavior, Corros. Commun. 20 (2025) 33–41.
[24] N. Du, X. Li, X. Wei, et al., Atomistic insights into interfacial optimization mechanism for achieving ultralow-friction amorphous carbon films under solid–liquid composite conditions, ACS Appl. Mater. Interfaces 15 (45) (2023) 53122–53135.
[25] N. Du, X. Li, X. Wei, et al., Comprehensive optimization of friction performance of amorphous carbon films under complex solid–liquid composite conditions, Appl. Surf. Sci. 688 (2025) 162468.
[26] S. Alavi, J.A. Ripmeester, D.D. Klug, Molecular-dynamics study of structure II hydrogen clathrates, J. Chem. Phys. 123 (2) (2005) 24507.
[27] N. Xu, C. Wang, L. Yang, et al., Nano-scale coating wear measurement by introducing Raman-sensing underlayer, J. Mater. Sci. Technol. 96 (2022) 285–294.
[28] A.P. Thompson, H.M. Aktulga, R. Berger, et al., LAMMPS - a flexible simulation tool for particle-based materials modeling at the atomic, meso, and continuum scales, Comput. Phys. Commun. 271 (2022) 108171.
[29] A. Rajabpour, B. Mortazavi, P. Mirchi, et al., Accurate estimation of interfacial thermal conductance between silicon and diamond enabled by a machine learning interatomic potential, Int. J. Therm. Sci. 214 (2025) 109876.
[30] X. Li, A. Wang, K. Lee, Comparison of empirical potentials for calculating structural properties of amorphous carbon films by molecular dynamics simulation, Comput. Mater. Sci. 151 (2018) 246–254.
[31] X. Li, P. Ke, H. Zheng, et al., Structural properties and growth evolution of diamond-like carbon films with different incident energies: a molecular dynamics study, Appl. Surf. Sci. 273 (2013) 670–675.
[32] X. Li, P. Ke, K. Lee, et al., Molecular dynamics simulation for the influence of incident angles of energetic carbon atoms on the structure and properties of diamond-like carbon films, Thin Solid Films 552 (2014) 136–140.
[33] F. Tavazza, T.P. Senftle, C. Zou, et al., Molecular dynamics investigation of the effects of tip–substrate interactions during nanoindentation, J. Phys. Chem. C 119 (24) (2015) 13580–13589.
[34] X. Wei, N. Du, P. Guo, et al., Friction dependence on processing priority for graphitization/passivation coupled amorphous carbon films, Carbon 230 (2024) 119631.
[35] X. Li, N. Du, C. Feng, et al., Theoretical superlubricity and its friction stability of amorphous carbon film induced by simple surface graphitization, Appl. Surf. Sci. 615 (2023) 156318.
[36] N. Du, X. Wei, X. Li, et al., Friction reactions induced by selective hydrogenation of textured surface under lubricant conditions, Friction 12 (1) (2024) 174–184.
[37] H.J.C. Berendsen, J.P.M. Postma, W.F. van Gunsteren, et al., Molecular dynamics with coupling to an external bath, J. Chem. Phys. 81 (8) (1984) 3684–3690.
[38] W.D. Nix, B.M. Clemens, Crystallite coalescence: a mechanism for intrinsic tensile stresses in thin films, J. Mater. Res. 14 (8) (1999) 3467–3473.
[39] C.A. Davis, A simple model for the formation of compressive stress in thin films by ion bombardment, Thin Solid Films 226 (1) (1993) 30–34.
[40] N. Du, Y. Wang, X. Wei, et al., Low-stress optimization and enhanced tribological properties of multilayer DLC films via alternating-energy deposition[J], Carbon 244 (2025) 120721.
[41] A. Stukowski, Visualization and analysis of atomistic simulation data with OVITO–the open visualization tool, Model. Simul. Mater. Sci. Eng. 18 (1) (2010) 15012.
[42] M. Moseler, P. Gumbsch, C. Casiraghi, et al., The ultrasmoothness of diamond-like carbon surfaces, Science 309 (5740) (2005) 1545–1548.
[43] N.A. Marks, Thin film deposition of tetrahedral amorphous carbon: a molecular dynamics study, Diam. Relat. Mater. 14 (8) (2005) 1223–1231.
[44] T. Ma, Y. Hu, H. Wang, Molecular dynamics simulation of the growth and structural properties of ultra-thin diamond-like carbon films, Acta Phys. Sin. 55 (6) (2006) 2922–2927.
[45] Y. Wang, K. Hayashi, Y. Ootani, et al., Role of OH termination in mitigating friction of diamond-like carbon under high load: a joint simulation and experimental study, Langmuir 37 (20) (2021) 6292–6300.
[46] L. Bai, N. Srikanth, E.A. Korznikova, et al., Wear and friction between smooth or rough diamond-like carbon films and diamond tips, Wear 372 (2017) 12–20.
[47] Z. Chen, N. Du, X. Li, et al., Atomic-scale understanding on the tribological behavior of amorphous carbon films under different contact pressures and surface textured shapes, Materials 16 (18) (2023) 6108.
[48] S. Li, X. Yang, Y. Kang, et al., Progress on current-carry friction and wear: an overview from measurements to mechanism, Coatings 12 (9) (2022) 1345.
[49] W. Shao, Z. Shi, L. Rao, et al., High-temperature sliding friction behavior of amorphous carbon films: molecular dynamics simulation, Langmuir 36 (50) (2020) 15319–15330.
[50] Y. Wang, N. Yamada, J. Xu, et al., Triboemission of hydrocarbon molecules from diamond-like carbon friction interface induces atomic-scale wear, Sci. Adv. 5 (11) (2019) eaax9301.